

The role of step collisions on diffraction from vicinal surfaces

N.C. Bartelt, T.L. Einstein and Ellen D. Williams

Department of Physics, University of Maryland, College Park, MD 20742-4111, USA

Received 20 November 1991; accepted for publication 6 May 1992

To assist efforts to extract information about the energetics of step structure from measured diffraction profiles, we have used Monte Carlo simulations to compute correlation functions and diffraction profiles of the terrace–step–kink model of vicinal surfaces. We compare the results to the predictions of simple scaling arguments. We concentrate on the temperature dependence of correlations along the average step–edge direction. These correlations are well-known to reflect the (sometimes strong) temperature dependence of the mean distance between step–step collisions, y_{coll} . Our calculations show explicitly how y_{coll} governs the behavior of correlations parallel to the step edge. For example, only at length scales larger than y_{coll} can one observe the well-known logarithmic divergence in surface height correlations, and the consequent power-law lineshape of the structure factor. (For large momentum transfer (short length scales), we find a Lorentzian component in the structure factor with a width proportional to the mean collision distance.) We discuss the feasibility of estimating kink energies from the temperature dependence of diffraction profiles. By scaling the profiles at different temperatures and/or misorientations, one can extract variations in y_{coll} and thence the step–edge stiffness. Finally, we discuss how energetic interactions between steps influence diffraction features such as line shapes, spot anisotropies, and scaling properties. Comparison is made with recent experiments on Si(111).

1. Introduction

Steps on surfaces play an important role in many significant and interesting surface processes [1]. Despite this importance, in general there is little quantitative information available about the factors governing step structure. A primary purpose of this paper is to assess what information can be learned about vicinal surfaces from diffraction measurements. We have attacked this problem by first analyzing analytically the various limiting regimes of behavior on the basis of simple approximations and then using Monte Carlo to directly compute the temperature dependence of the diffraction pattern from the simple terrace–step–kink model of stepped surfaces in thermal equilibrium, to corroborate this analysis and to determine where the transitions between regimes occur.

Recently, direct information about the energetics of step structure has been obtained by scanning tunnelling microscopy (STM) measure-

ments of step meanderings. For example, Swartzentruber et al. [2] have determined the details of the kink Hamiltonian on vicinal Si(001); in particular, they determined the kink energy as a function of kink size. One of the principal points of our paper is that such details of step structure are *not* readily available from diffraction measurements. For example, we will show that different kink Hamiltonians giving rise to similar orientational dependence of the step free energy will have similar diffraction patterns. To estimate the parameters of the kink Hamiltonian, one must hypothesize a microscopic model of the step free energy.

Given the authoritative nature of the STM work, we must offer an explanation for bringing up the old problem of interpreting diffraction measurement of stepped surfaces. Unfortunately, it is not yet generally possible to operate an STM at the temperatures at which Si surfaces have sufficient mobility to achieve equilibrium [3]. Analyses at room temperature consequently assume that they

are probing a quenched record of the equilibrium distribution associated with a much higher temperature [2,4]. In order to assess the validity of this assumption, as well as the reversibility of behavior as a function of temperature (a fundamental requirement of equilibrium), it is important to have a probe which operates at such high temperatures. Widely employed in studies of vicinal surfaces, diffraction probes, using electrons [5–8], X-rays [9], or helium [10,11], have this capability. Another advantage of diffraction techniques is that it is often very difficult to use STM during crystal growth, when the role of steps is particularly important.

A considerable amount of work has already been devoted to understanding diffraction from stepped surfaces [12,13]. For example, it is well-known by the analogy of steps on vicinal surfaces to domain walls in incommensurate phases [9,14–16] that the diffraction profiles will have a power-law shape over at least some range of small momentum transfer. Our work is similar in spirit to that of Selke et al. [13] for high-Miller-index surfaces near their roughening temperature: however, our concern is for systems with steps which are so far apart that step–step interactions are small; these systems are thus normally far above their roughening temperature. The thermal behavior is much simpler here, and so we are able to discuss the step correlation functions and diffraction pattern fairly simply and generally in terms of elementary step properties. We also discuss more thoroughly the breakdown of the logarithmic form of the step correlation functions at small distances (a breakdown which arises because of the large distances between steps, and which is not so evident (or important) on high-index surfaces). Much of the understanding of steps which are far apart comes from the analogy of steps or domain walls with free fermions [15,17,18]. Rather than taking the free fermion approach to computing correlation functions (which can become quite complex when computing diffraction profiles [18]), we here primarily use the Monte Carlo method. Since the free fermion analogy is usually only exact in the limit of small temperatures and widely distant non-interacting steps, the Monte Carlo approach has the advan-

tage of showing explicitly to what extent the free fermion concepts are realized in microscopic models of real surfaces.

In a previous study [8], we used Monte Carlo simulations to verify the expectation that in the direction perpendicular to the step edges (as with the case for closely-spaced steps [13]), the power-law profiles accurately describe profiles for a large k region. Moreover, we showed that the lineshape in this direction has only a weak thermal dependence (now in *contrast* to the case of closely-spaced, interacting steps), related to the observation that the characteristic length in this direction is the average spacing between steps, explored solely by the misorientation angle. In this paper, we present analogous results for the diffraction profiles parallel to the average direction of the step edges, perpendicular to the misorientation direction. We explicitly show, as suggested by the analysis of refs. [17,19], that the results can be simply interpreted in terms of the sizeable temperature dependence of the mean distance between step collisions along this direction. Indeed, this distance sets the characteristic length for essentially all dependencies on spacings in this transverse direction; in particular, we show how in the absence of interactions both the mean-square deviation and the transverse structure factor accurately satisfy scaling relations in which this distance serves as the distance scale. Conversely, any attempt to analyze the temperature dependence of such non-microscopic data will yield this characteristic length or equivalently, the diffusivity or meandering probability of the step, rather than a direct measurement of the kink energy, as we shall explain.

Most of our computational work is based on the venerable [20] terrace–step–kink model, which is illustrated in fig. 1. This model neglects adatom or vacancy excitations on the terraces. In a simple formulation, a kink of length na_{\perp} costs energy $|n|\epsilon$: the configuration shown is from a Monte Carlo simulation at $k_B T = \epsilon$. With increasing temperature, step meandering increases [21–23]. The qualitative sensitivity of the diffraction pattern to this meandering is shown in fig. 2, which previews results of the Monte Carlo calculations discussed below. At the presented “out-

of-phase” condition, the diffraction pattern consists of a “split beam” with splitting $2\pi/l$ in the direction perpendicular to the step edges [5], where l is the average spacing between steps. While the splitting remains well-resolved with increasing temperature (because the profiles perpendicular to the step edges have only a weak temperature dependence [8] in this model), there is considerable broadening in the transverse (\hat{y}) direction. This broadening is the subject of this paper.

The plan of the paper is as follows. In the next section we discuss the real-space correlation functions characterizing the meanderings of a step. Considering the mean-square displacement of the step perpendicular to the average direction of step “propagation,” we note three regimes of different simple behavior as a function of separation along this average direction. To understand the behavior of the steps at small distances (and,

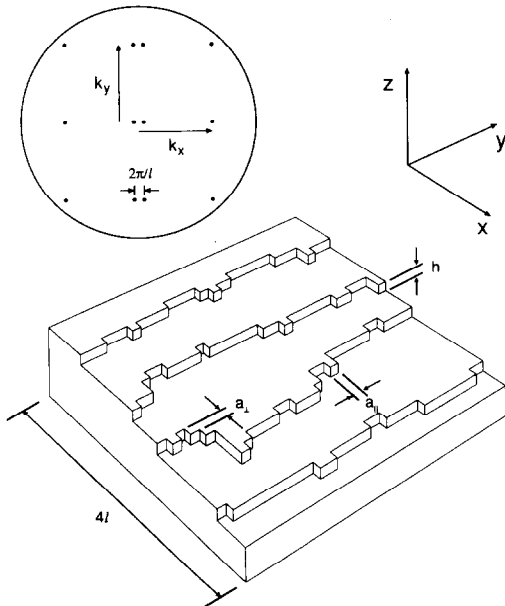


Fig. 1. Sample Monte Carlo configuration of the terrace step kink (TSK) model of a vicinal surface at a temperature equal to the kink energy. The coordinate system used in this paper is also shown. The inset shows a schematic of the corresponding diffraction pattern showing split beams at out-of-phase conditions, i.e., when the difference in path length for scattering from adjacent terraces equals an odd number of half-wavelengths, e.g., $k_z = \pi/h$.

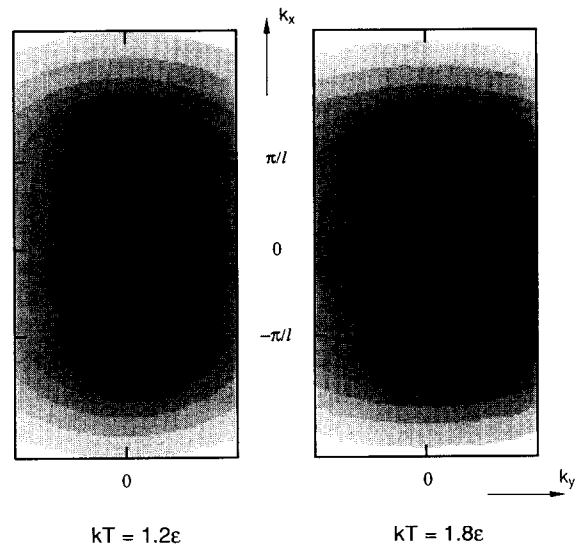


Fig. 2. Logarithmic grey scale images of the simulated diffraction pattern of stepped surfaces in the TSK model shown in fig. 1, at three different temperatures. These contour plots illustrate the effect discussed in this paper: increasing the temperature increases the step wandering and the width of the beams transverse to the step direction. This pattern is at an out-of-phase condition, i.e., $k_z = \pi/h$.

thus, the lineshape at large Δk), we approximate this system by a single step trapped between two straight steps – a model introduced by Gruber and Mullins [21]. When the steps are sufficiently far apart, the correlations can be simply and accurately computed within this model by drawing upon the analogy between the wandering step and a quantum mechanical particle trapped in a one-dimensional well [22,23]: the transverse structure factor can be expressed in terms of the eigenstates and eigenfunctions of Schrödinger’s equation for a particle in a box. As we discuss in detail below, comparison of the properties of the simple Gruber–Mullins model with those found from the more general computations show good *quantitative* agreement for small y or large momentum transfer. We then discuss the change in behavior that occurs at the length scale of the step collision distance and show how the collision distance depends on the kink energy and on temperature. We define the diffusivity (or, alternatively, the inverse step-edge stiffness) as a key concept and relate it to a measure of the effective

distance between close approaches of neighboring steps. We emphasize how this distance sets the length scale of behavior in this direction. In the third section, we perform a similar analysis of the structure factor. We show that scaling arguments can be applied to describe diffraction profiles, again with an emphasis on the step collision distance. Both the anisotropy of line profiles and the deviations of the line shape from power-law form are discussed in terms of the collision distance. In the fourth section, changes in the step collision distance caused by energetic step-step interactions and the resulting changes in the correlation functions and line profiles are discussed. We find that knowledge of the step-edge stiffness and the terrace width distribution enable one to make a reasonable estimate of the shape of the diffraction profiles. This estimate is discussed in the context of recent diffraction and microscopy measurements on vicinal Si(111). We conclude with a discussion of feasibility of analysis of experimental data based on these ideas, to evaluate the step collision distance, and thence the kink energy.

2. Step-position correlation functions: mean-square displacements

As a prelude to our discussion of the transverse structure factor, in this section we describe the behavior of the real-space correlations along a single step edge. In particular, we consider the mean-square displacement as a function of distance y along the step edge:

$$g_x(y) \equiv \langle [x(y) - x(0)]^2 \rangle, \quad (1)$$

where $x(y)$ charts the course of one step edge [24], as shown in fig. 1. This correlation function can be used directly for analyzing data from stepped surfaces obtained by STM [2,4], reflection electron microscopy [25], or low-energy electron microscopy [26].

Since we assume no interaction between kinks on the same step, the probability of a particular configuration of a single *isolated* step can be simply written as a product of probabilities of

each kink: the step edge represents a simple random walk [22]. In a random walk, the key parameter which scales the amount of meandering is the step edge “diffusivity” $b^2(T)$, i.e., the mean-square perpendicular deviation with each pace “forward” [1,8,23]. At small y , the behavior of $g_x(y)$ is particularly simple^{#1}. Here the approximation of isolated steps is valid, so that the mean-square displacement is proportional to the number of “paces” in the walk:

$$g_x(y) \sim b^2(T)y/a_{\parallel}. \quad (2)$$

To compute b^2 from microscopic interactions, we need to know $E(n)$, the energy of a kink of size n , i.e., a move in the $\pm\hat{x}$ direction of size na_{\perp} . Then b^2 is given by the simple Boltzmann-weighted average over all possible values of the kink size:

$$b^2(T) = \frac{2a_{\perp}^2 \sum_{n=1}^{\infty} n^2 \exp[-E(n)/k_{\text{B}}T]}{1 + 2 \sum_{n=1}^{\infty} \exp[-E(n)/k_{\text{B}}T]}. \quad (3)$$

Thus, b^2 is usually a monotonically increasing function of T . As reviewed below, we emphasize that *the only way that the kink energy $E(n)$ enters the macroscopic physics is through the diffusivity*. Conversely, analysis of diffraction data or other macroscopic measurements as a function of T will only yield $b^2(T)$; to go the last step to $E(n)$ requires some knowledge or assumption of the form of $E(n)$.

To gauge the sensitivity of $b^2(T)$ to assumptions about the form of $E(n)$, we consider some typical examples and collect the results in table 1. In the TSK model, $E(n)$ is just proportional to the length of a kink. In analyzing the meandering of “ S_{B} ” steps of (2×1) -reconstructed vicinal Si(100), Swartzentruber et al. found that a “corner energy” ϵ_c [2,27] was also evident, providing an

^{#1} The analogy of steps with random walkers can be fruitfully extended to the case when steps collide, as elegantly described in ref. [22]. Since one must drop configurations from the ensemble averages which contain steps which cross, the appropriate random walkers are “vicious” (rather than “bouncy”).

Table 1
Temperature dependence of b^2 for the various kink Hamiltonians discussed in the text

| Model | $E(n)$ | b^2/a_{\perp}^2 |
|-------------------|--|--|
| TSK | $ n \epsilon$ | $\frac{1}{2} \sinh^{-2}(\epsilon/2k_{\text{B}}T)$ |
| TSK + corner | $ n \epsilon + (1 - \delta_{n,0})\epsilon_c$ | $b_{\text{TSK}}^2 / \{1 + [\exp(\epsilon_c/k_{\text{B}}T) - 1] \tanh(\epsilon/2k_{\text{B}}T)\}$ |
| Discrete Gaussian | $n^2\epsilon$ | Not a simple function |
| Restricted | $E(0) = 0, E(\pm 1) = \epsilon$ | $2/[2 + \exp(\epsilon/k_{\text{B}}T)]$ |

additional constant contribution whenever there was a kink. Specifically in this case $\epsilon_c \approx 3\epsilon$. For theoretical analysis, it often is easier to use models which restrict large kinks relatively more severely, with the expectation that the general features should not be altered. These sorts of approximations, made in the \hat{z} direction, were used to characterize the roughening transition [28,29]. For example, in the discrete Gaussian model [28], the kink energy depends quadratically on its size. More severely, one can invoke “restricted” models [29], in which the step can wander by at most a_{\perp} , i.e. $E(1) = \epsilon$ and $E(n \geq 2) = \infty$. At low temperatures in all cases b^2/a_{\perp}^2 is equal to $\exp(-E(1)/k_{\text{B}}T)$, which in turn is proportional to the kink density. As can be seen from the plots of $b^2(T)$ for these various cases in

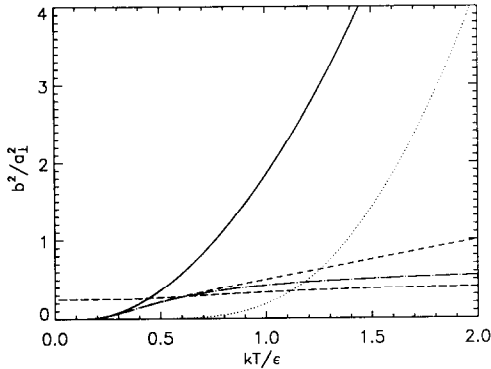


Fig. 3. Temperature dependence of $b^2 \propto y_{\text{coll}}$, for the four cases discussed following eq. (3): (a) solid curve: TSK model, in which a kink of length na_{\perp} costs energy $E(n) = |n|\epsilon$; (b) dotted curve: TSK model with an additional corner energy 3ϵ ; (c) short dashed curve: discrete Gaussian model, $E(n) = n^2\epsilon$; (d) dash-dotted curve: restricted model, with only $n = 0, 1$ allowed; (e) long-dashed curve: restricted model in which the step is misoriented away from the high-symmetry direction (eq. (20)).

fig. 3, a poor assumption about the form of $E(n)$ can lead to a value of ϵ that is incorrect by as much as an order of magnitude or more. The high-temperature limits of all of these models are unrealistic because of the neglect of overhangs and adatom and vacancy excitations on the terraces.

As an aside to prevent possible confusion, we note that while most step displacement correlation functions exhibit logarithmic behavior at large separation (because these surfaces are technically “rough”), the behavior at small y may differ considerably. For example, the seemingly similar height correlation function analyzed by Villain et al. [12]

$$g_z(y) \equiv \langle [z(y) - z(0)]^2 \rangle \sim \frac{bh^2}{l} \sqrt{\frac{2y}{\pi a_{\parallel}}} \quad (4)$$

at small y , as we show in the appendix.

When the steps begin to collide, i.e., when the mean-square displacement becomes a significant fraction of the terrace width, deviations from linear, “diffusive” behavior must occur. To understand the temperature dependence at these distances, we draw on heuristic arguments rationalizing the analogous behavior of domain walls in incommensurate phases. The key idea is that the characteristic length which determines $g_x(y)/l^2$ is the average distance from any point on a step edge to a point where this step collides with (i.e., comes within a_{\perp} of) an adjacent step [19,17,22,30]. One expects this collision distance to be the distance y along the step edge required for an isolated step to wander a distance $l/2$ in the direction x perpendicular to the step edge. Guided by eq. (2), we thus define the collision distance

$$y_{\text{coll}} = l^2 a_{\parallel} / 4b^2. \quad (5)$$

For $l = 16$ and $k_B T = 1.4\epsilon$, y_{coll} is $\sim 17 a_{\parallel}$ in the simple TSK model.

The simplest scheme to account for collisions with neighboring steps is the Gruber–Mullins model. In this approximation, the problem is reduced to that of a single wandering wall between two straight fixed walls separated by twice the average interstep separation, $2l$. As we next show, a convenient way of estimating the correlation functions for this model is to take the continuum limit in the \hat{y} direction, which reduces the problem to solving the 1D Schrödinger’s equation for a quantum mechanical particle in a box.

Consider a segment of the step from dy to $y + dy$ along the step edge. There are dy/a_{\parallel} possible kinks. From the central limit theorem, one expects the probability distribution for the step to wander a distance dx during this length to be approximately Gaussian with a second moment proportional to the number of kink sites multiplied by the second moment of the kink distribution at each kink site (cf. eq. (2)), i.e.,

$$P(x, x + dx; y, y + dy) \propto \exp\left(-\frac{a_{\parallel}}{2b^2} \frac{(dx)^2}{dy}\right), \quad (6)$$

so that the probability of a particular step configuration $x(y)$ is

$$P(x(y)) \propto \exp\left(-\frac{a_{\parallel}}{2b^2} \int \left(\frac{dx}{dy}\right)^2 dy\right). \quad (7)$$

Using standard path-integral arguments [1,5,31] the probability of a step passing through x at y and x' at y' can be written as

$$P(x, x'; y, y') = \sum_s \exp[-(E_s - E_0)|y' - y|] \times \psi_0^*(x) \psi_0(x') \psi_s^*(x') \psi_s(x), \quad (8)$$

where the ψ_s ’s are the eigenstates of Schrödinger’s equation:

$$-\frac{b^2}{2a_{\parallel}} \frac{d^2 \psi_s}{dx^2} = E_s \psi_s, \quad (9)$$

and where $s = 0$ denotes the ground state and the eigenvalues $E_s = b^2 \pi^2 (s + 1)^2 / 8a_{\parallel} l^2$ are energies per unit length.

Because we assume that the wandering step cannot pass through the neighboring straight steps, we require that the ψ_s go (continuously) to zero at $x = \pm l$: we use the familiar sinusoidal wavefunctions for a particle trapped between two impenetrable walls. Recognizing that $g(y, y') \equiv g(|y - y'|)$ is just the double integral of $(x - x')^2$ weighted by $P(x, x'; y, y')$, eq. (8) then gives a simple expression for the mean-square displacement (in which only terms with $s = 2p - 1$ survive):

$$\frac{g_x(y)}{l^2} = 2 \left(\frac{w_{\text{GM}}}{l}\right)^2 - \frac{2048}{\pi^4} \sum_{p=1}^{\infty} \frac{p^2}{(4p^2 - 1)^4} e^{-y/\xi_p}, \quad (10)$$

where

$$\left(\frac{w_{\text{GM}}}{l}\right)^2 = \frac{2}{\pi^2} \left(\frac{\pi^2}{6} - 1\right) \approx 0.131 \quad (11)$$

and

$$\xi_p = \frac{8l^2 a_{\parallel}}{(4p^2 - 1)\pi^2 b^2} = \frac{3\xi_1}{4p^2 - 1}. \quad (12)$$

In general only the first term in the summation is needed, and $g(y)$ is seen to approach, from below with simple exponential decay, a constant simply related to the root-mean-square deviation w_{GM} of the step from half-way between the two fixed boundaries in the Gruber–Mullins model. The flattening out of $g_x(y)$ with increasing y is clearly an artifact of this fixed-wall approximation. Notice that ξ_1 contains the same parameters as y_{coll} , differing only by the numerical factor $32/3\pi^2 \approx 1.08$. For small y , all terms must contribute to reproduce the linear behavior noted earlier. (Furthermore, expansion around $y = 0$ recovers eq. (2).)

We can go beyond the Gruber–Mullins approximation to explore “many-wall” aspects of the problem by using the free-fermion approximation. For large y the form of $g_x(y)$ (in the

absence of energetic interactions between the steps, or at sufficiently high temperature) is expected to be given by [8,12,18,32]

$$g_x(y) \sim \frac{2l^2}{\pi^2} \eta \ln(y). \quad (13)$$

This behavior can occur only on length scales larger than the step collision distance y_{coll} . In the absence of energetic interactions, the analogy of steps with free fermions [17,18,32] yields the prediction that η is $\frac{1}{2}$ in the asymptotic limit of vanishing misorientation, i.e., infinite l and y (independent of T !).

To corroborate these ideas, we computed $g_x(y)$, normalized to the square of the average terrace width, for several temperatures, using standard Monte Carlo techniques. The lattice had an average terrace size $l = 16a_{\perp}$, with 32 steps established by screw periodic boundary conditions in the \hat{x} direction; each extended $256a_{\parallel}$ in the \hat{y} direction (with periodic boundary conditions in that direction). Typically 10^7 Monte Carlo steps per step site were used; 10^6 Monte Carlo steps were allowed for equilibration. The raw results are displayed in fig. 4.

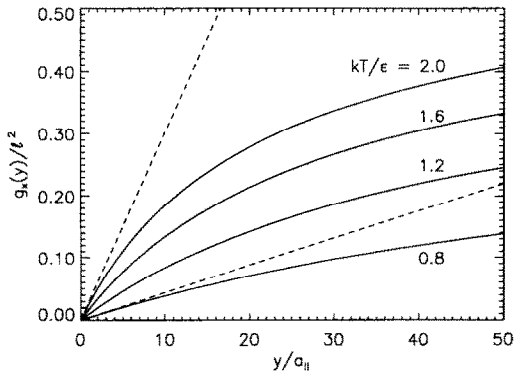


Fig. 4. Mean-square displacement, g , as a function of the distance y along a step for four temperatures. y is measured in units of a_{\parallel} ; g_x is normalized by l^2 . For the highest and the lowest depicted temperatures, 2.0 and 0.8 ϵ/k_B , dashed lines show the limiting diffusive behavior of eq. (2), which evidently holds only at small y . This plot and most subsequent ones were computed using a lattice with 32 steps, $l = 16a_{\perp}$ in the \hat{x} direction and periodic boundary conditions with $256a_{\parallel}$ in the \hat{y} direction. Typically 10^7 Monte Carlo steps per site were used in computing these curves (with the first 10^6 discarded for equilibration).

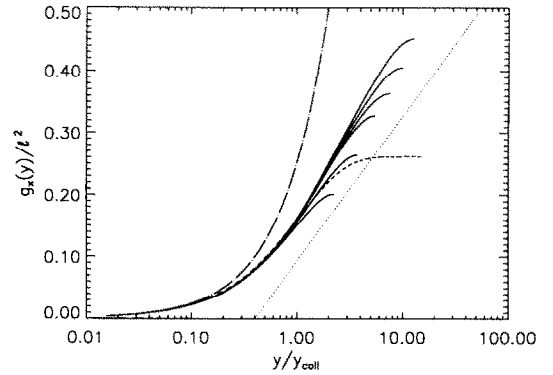


Fig. 5. When the data of fig. 4 is rescaled by dividing y by y_{coll} , the data collapses onto a single curve. At larger y there is a region of effective logarithmic divergence of g . The dashed line shows the prediction of the Gruber–Mullins model (eq. (10)). The dotted line has a slope corresponding to eq. (13) with $\eta = 0.5$. The dash-dotted curve shows the diffusive limit of eq. (2).

The initial linear increase of $g_x(y)$ is evident in fig. 4; for the highest and the lowest temperature displayed, the linear form given in eq. (2) is co-plotted for comparison. It is also clear that particularly as temperature increases, step collisions quickly become important. The exponential approach toward a constant for intermediate y , predicted in the Gruber–Mullins approximation, is also evident in the solid curves, as well as the eventual logarithmic divergence.

To highlight the key idea that the (only) characteristic distance in the \hat{y} direction is y_{coll} , we replot in fig. 5 the computed data in fig. 4 as a function of $\log(y/y_{\text{coll}})$. The most striking observation is how well the data from different temperatures scale until the largest values of y , at which finite-size effects introduce a new length which destroys the scaling: the periodic boundary conditions restrict the size of $g_x(y)$ when y gets close to 128. From eq. (2) it is clear that the expression for the linear regime obeys the scaling with y_{coll} ; this curve is included in fig. 5 for comparison. At small y , we see that deviations from diffusive behavior become noticeable once $y \approx 0.1y_{\text{coll}}$, and the somewhat more complicated Gruber–Mullins form of eq. (10) is needed. We see that this expression also scales explicitly with y_{coll} and is a good approximation until y gets

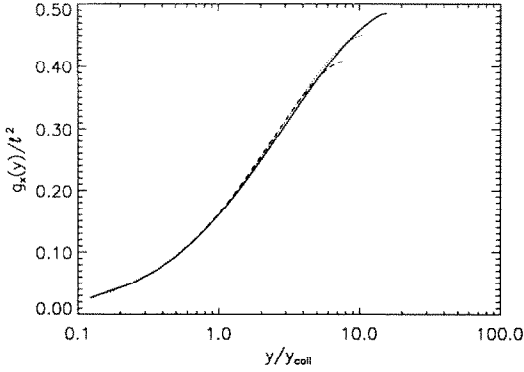


Fig. 6. Plot of $g_x(y)$ versus y/y_{coll} for $l=16$ (solid), 8 (dotted), and 6 (dashed), with $k_B T/\epsilon = 2.0, 1.2,$ and $0.8,$ respectively, to show that data for various terrace widths can also be collapsed by the scaling formulation. (Cf. eq. (5).)

somewhat larger than y_{coll} . The significance of this agreement for the form of the diffracted profiles will be discussed in the next section. For larger y , the logarithmic divergence expressed in eq. (13) occurs. Indeed, the plot of $g_x(y)$ versus $\log(y)$ of fig. 5 is approximately linear when $y/y_{\text{coll}} > 1$ (and before the onset of finite-size effects). The dotted line in the figure has a slope corresponding to the predicted limiting value $\eta = \frac{1}{2}$. At high temperatures, when b becomes a sizable fraction of l , fig. 5 provides some evidence that η becomes greater than 0.5. (For reference, b/l is ~ 0.2 for $k_B T = 1.8\epsilon$, the largest temperature on figs. 4 and 5.) Similar results are found in the \hat{x} direction [8,33].

In normalizing $g_x(y)$ by l^2 in figs. 4 and 5, we have implicitly recognized that l sets the scale for behavior in the \hat{x} direction, as discussed thoroughly elsewhere [8,23,34]. Moreover, l plays an important role in the \hat{y} direction by setting the deviation distance for a step to collide with its neighbor. To check further the scaling ideas, we show in fig. 6 that data for different l 's can also be collapsed onto a single curve by rescaling y with y_{coll} . Notice that even for l as small as $6a_{\perp}$, the rescaling works well. (In general one expects the rescaling to be successful as long as b^2 is much smaller than l^2 [23].)

None of the scaling features of the correlation functions depends on the microscopic details of

the kink Hamiltonian or the symmetry of the surface. To make this point clear, we consider the generalization to non-high symmetry directions, where there is a finite density of ‘‘kinks,’’ even at zero temperature. To determine b^2 as a function of temperature and net step orientation, it is convenient to introduce a kink chemical potential μ . Since we have assumed that the kinks do not interact with each other, the grand partition function of a step edge can be written as the product of the partition function q at each kink site:

$$q(T, \mu) = \sum_n \exp\{[-E(n) + \mu n]/k_B T\}. \quad (14)$$

The generalized Gibbs free energy per kink site is simply $g = -k_B T \ln(q)$. The mean-square size of each kink site can simply be obtained from g through

$$b^2 = -a_{\perp}^2 k_B T \frac{\partial^2 g}{\partial \mu^2}. \quad (15)$$

We wish to determine the dependence of the b^2 on step orientation $\rho \equiv a_{\perp} \langle n \rangle / a_{\parallel} = \tan(\theta)$ rather than μ . This density can be computed from g using

$$\rho = -\frac{a_{\perp}}{a_{\parallel}} \frac{\partial g}{\partial \mu}. \quad (16)$$

Eq. (15) can now be re-expressed in terms of derivatives with respect to ρ by introducing the Helmholtz free energy per kink site, $f = g + \mu\rho$:

$$b^2 = a_{\parallel}^2 k_B T \left(\frac{\partial^2 f}{\partial \rho^2} \right)^{-1}. \quad (17)$$

In terms of the free energy per unit length $\gamma(\theta)$ of the step edge (rather than per projected length, as in f), this can also be written in the more familiar form

$$\frac{a_{\parallel} k_B T}{b^2 \cos^3 \theta} = \tilde{\gamma} = \gamma + \frac{\partial^2 \gamma}{\partial \theta^2}, \quad (18)$$

where $\tilde{\gamma}(\theta)$ is the step-edge ‘‘stiffness’’ [35]. Eq. (18) leads to another way of expressing eq. (2) in terms of $\tilde{\gamma}$:

$$g_{x'}(y') = \frac{k_B T}{\tilde{\gamma}} y', \quad (19)$$

where x' and y' are coordinates perpendicular and parallel, respectively, to the average step edge. Eq. (19) is actually more general than eq. (2). If, for example, kinks at different sites are no longer independent, if there are overhangs in the step edge, or if terrace excitations exist, then eq. (19) should be used rather than eq. (2) ^{#2}.

For a model in which each kink is restricted to be at most one lattice constant long ^{#3}, one can show, using eqs. (14)–(18), that b^2 is just

$$\frac{b^2}{a_{\perp}^2} = \frac{4z_0^2 - \sqrt{\rho^2 + 4z_0^2(1 - \rho^2)}}{4z_0^2 - 1} - \rho^2, \quad (20)$$

where $z_0 = \exp(-\epsilon/k_B T)$. The curve showing b^2 when $\rho = 0.5$ is compared with the results for the high-symmetry directions in fig. 3. The distinctive feature of this curve is that b^2 does not vanish as the temperature approaches zero. This feature is

^{#2} Eq. (19) underscores the artificiality of using the models for b^2 of fig. 3 to predict step correlations at high temperature: On general grounds if one includes overhangs and terrace excitations, one expects the step free energy γ eventually to become isotropic and finally to vanish as the temperature is raised [35]. This behavior does not occur in the models considered here.

^{#3} The generalization of eq. (20) for the unrestricted TSK model is $b^2/a_{\perp}^2 = \rho^2 + \{h(\rho^2) + A[(1 + \rho^2)h(\rho^2) - A^2\rho^2]^{1/2}\}/\{A^2 - h(\rho^2)\}$, where $A = 1 + z_0^2$ and $h(\rho^2) = 4z_0^2 + (A^2 + A)\rho^2$.

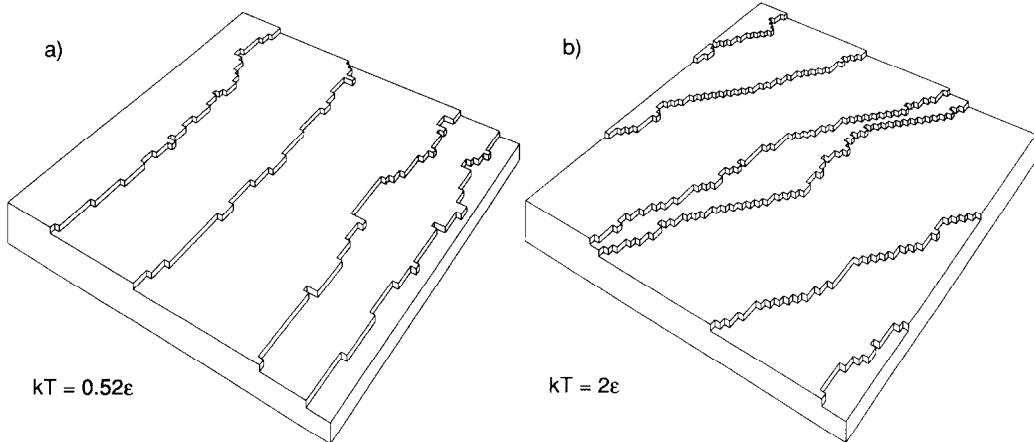


Fig. 8. (a) Picture of a stepped surface with the kink Hamiltonian $E(n) = |n|\epsilon$ at temperature of 0.52ϵ . (b) Stepped surface where the average step direction is rotated from the high symmetry direction of (a). In this model only kinks of length of one unit are allowed: the temperature is twice the kink energy ϵ .

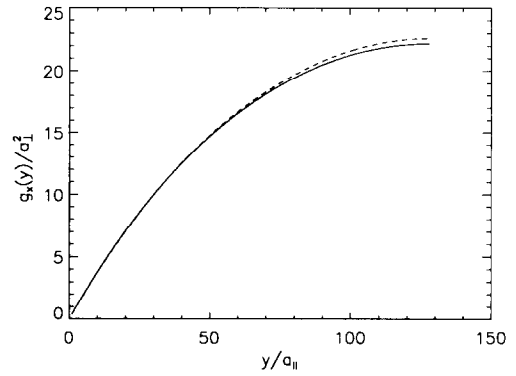


Fig. 7. Plot of $g_x(y)$ for the two step configurations pictured in figs. 8a (dashed) and 8b (solid). Despite the fact that the local step (kink) structure is completely different in the two cases, b^2 (or the step stiffness) and the average terrace width is the same for both cases and hence the correlation functions of the two cases are quite similar.

a consequence of the fact that even at zero temperature there is randomness in the positions of the kinks (because of the assumption of no kink–kink interactions). Now, to convince the reader that correlation functions along the step edge depend primarily on the value of b^2 (or, more generally, on $\tilde{\gamma}$), fig. 7 compares $g_x(y)$ for two systems with distinctly different kink structures but the same b^2 . The first case, pictured in fig. 8a, is the unrestricted TSK model of the solid line

of fig. 3; the second (cf. fig. 8b) has the average step direction rotated by $\theta = \tan^{-1}(0.5)$ (long-dashed line of fig. 3). The differences between the two curves are small.

3. Diffraction from stepped surfaces

To calculate the transverse diffraction profiles, we assume the scattered intensity is given by the kinematic structure factor

$$S(k_x, k_y, k_z) = \left\langle \left| \sum_{(x, y, z)} \exp(i(k_x x + k_y y + k_z z)) \right|^2 \right\rangle. \quad (21)$$

In our model we include only the positions of the uppermost atoms in the summation. Since the scattered intensity is most sensitive to step structure when neighboring terraces scatter out-of-phase, we set $k_z = \pi/h$, in which case the peaks in scattered intensity pictured in fig. 2 occur at $k_x = \pm\pi/l$. Fig. 9 plots the logarithm of the transverse profile $S(k_y) = S(\pi/l, k_y, \pi/h)$ calculated from Monte Carlo data for the same range of temperatures shown in figs. 4 and 5. As the temperature is raised, the scattered intensity becomes progressively more diffuse as anticipated

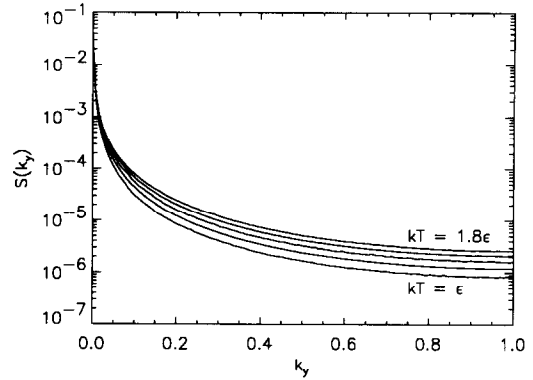


Fig. 9. Transverse structure factor, i.e., the profile along a vertical line in fig. 1 starting at the center of a split spot, for five temperatures within the range shown in fig. 4; k_y is in units of π/a_{\parallel} .

by fig. 2. The strong thermal dependence of the lineshape shown in fig. 9 contrasts with that perpendicular to the steps, which is much less sensitive to temperature [8].

To evaluate the thermal evolution of the lineshape, we again rescale distances by y_{coll} as done in fig. 5. From the dimensional arguments of the preceding section, one expects that correlation functions that depend on y and other variables like temperature and terrace width can be collapsed to “universal” functions of just $\tilde{y} \equiv y/y_{\text{coll}}$.

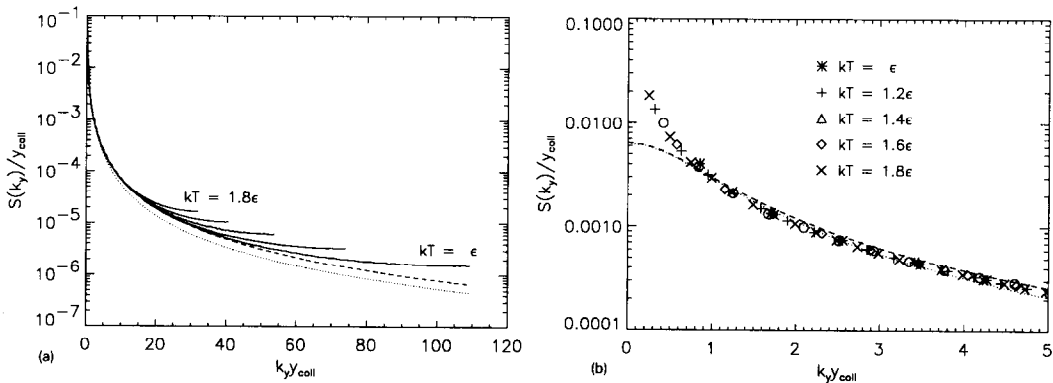


Fig. 10. (a) Illustration of how scaling collapses the structure factors for several temperatures onto a single curve. The solid lines show the scaled curves from fig. 9: each curve ends at the value of $k_y y_{\text{coll}}$ for which $k_y = \pi/a_{\parallel}$. The dashed line shows for comparison the Gruber–Mullins approximation of eq. (25); the dotted line shows the prediction of eq. (25) including only the $p = 1$ term, i.e., a single Lorentzian. (b) This plot expands the small k_y regime of (a), presumably the only region in which the intensity is sufficiently strong to permit reliable experimental measurements.

In particular, we expect that the transverse structure factor can be rescaled as follows:

$$S(k_y, T, l) = \int dy e^{ik_y y} f(y) \\ = y_{\text{coll}} \int d\tilde{y} e^{ik_y y_{\text{coll}} \tilde{y}} \mathcal{F}(\tilde{y}), \quad (22)$$

so that

$$S(k_y, T, l) = y_{\text{coll}}(l, T) \mathcal{Z}(k_y y_{\text{coll}}(l, T)), \quad (23)$$

where $\mathcal{Z}(\tau)$ is a universal function. (Note that in contrast to the analysis of the mean-square displacement, the value of S is also rescaled. Heuristically, because S is proportional to the area of the surface, dividing y by y_{coll} requires that S be proportional to y_{coll} .) In fig. 10a we recast the computed data of fig. 10 as a semi-log plot of \mathcal{Z} , i.e., $S(k_y, T, l)/y_{\text{coll}}(l, T)$, versus $k_y y_{\text{coll}}$. Fig. 10b highlights and enlarges the region near the center of a spot, where the intensity is great enough to permit accurate measurement. (Fig. 10b includes intensities down to 10^{-4} of that at the center of the spot, which is probably optimistic compared to current capabilities [9].) Again the scaling effectively collapses the data onto a single curve until large k_y becomes on the order of π/a_{\parallel} , $S(k_y)$ becomes sensitive to the atomic geometry of the kinks, and the scaling fails. The impressive scaling shows that the strong temperature dependence of $S(k_y)$ comes from the strong temperature dependence of the prefactor y_{coll} .

To understand the line shape at large momentum transfer, we use the fact (fig. 5) that $g_x(y)$ is accurately described by the Gruber–Mullins model for distances $y < y_{\text{coll}}$. We thus anticipate that at large momentum transfer, $S(k_y)$ is also well-approximated. To show this explicitly, we compute $S(k_y)$ for the Gruber–Mullins model. The requirement that each step be restricted to $-l < x < l$ allows eq. (21) to be written as

$$S(k_y) = \frac{1}{\pi^2} \left\langle \left| \int dy [1 + \exp(i\pi x(y)/l)] \right. \right. \\ \left. \left. \times \exp(ik_y y) \right|^2 \right\rangle. \quad (24)$$

Using eq. (8) to compute the expectation values, one finds that

$$S(k_y) = \frac{2}{\pi^4} \delta(k_y) \\ + \frac{1024}{\pi^4} \sum_{p=1}^{\infty} \frac{1}{(4p^2 - 1)^2 (4p^2 - 9)^2} \\ \times \left[\frac{(\xi_p)^{-1}}{k_y^2 + (\xi_p)^{-2}} \right], \quad (25)$$

where ξ_p was defined above in eq. (10). The δ function is a manifestation of the straight-boundary assumption of the model. It overestimates severely the intensity at $k_y = 0$, and will be henceforth ignored in comparisons with the Monte Carlo results. Eq. (25) is compared to the Monte Carlo data in fig. 10. (Notice again that the scaling of fig. 10 is implicit in the assumptions leading to eq. (25).) The curves agree well over the range of approximately $1/y_{\text{coll}} < k_y < \pi/2a_{\parallel}$. An approximate analytical form for $S(k_y)$ can be computed with just the $p = 1$ term of eq. (25). Over an intermediate regime of k_y ($1/y_{\text{coll}} < k_y < 2\pi/y_{\text{coll}}$), with is highlighted in fig. 10b and beyond which $S(k_y)$ is immeasurably small, the structure factor $S(k_y)$ is well described by this simple Lorentzian – represented by the dotted line in the figure – with correlation length given by

$$\xi(T, l) = \xi_1 = \frac{8a_{\parallel}}{3\pi^2} \left(\frac{l}{b(T)} \right)^2. \quad (26)$$

As noted following eq. (12), ξ_1 is almost identical to y_{coll} , as was anticipated by our definition of y_{coll} .

At small k_y previous work [8,12] has shown that when the height–height correlation function g_x diverges logarithmically, the scattered intensity for a specular beam at an out-of-phase condition has a power-law lineshape:

$$S(k_x, k_y) \\ = I_0 \left[\left(\frac{k_x \pm \pi/l}{c_x} \right)^2 + \left(\frac{k_y}{c_y} \right)^2 \right]^{-(2-\eta)/2}, \quad (27)$$

where η is given in eq. (13). However, in the \hat{y} direction, fig. 5 shows that the logarithmic approximation for real-space behavior fails at distances less than y_{coll} . Thus we expect – and observe in fig. 10b – a power law to describe the line shape in the \hat{y} direction only at small momentum transfer $k_y < 1/y_{\text{coll}}$, albeit in the regime where $S(k_y)$ is most readily observed. In fact, the transition from Lorentzian to power-law behavior occurs quite abruptly around $1/y_{\text{coll}}$. (By contrast, in the \hat{x} direction, perpendicular to the steps, we have showed explicitly (cf. fig. 5 of ref. [8]) that the correlation function $g_x(z, y)$ is approximately logarithmic even at small distances and thus the structure-factor profile in this direction is power-law for any momentum transfer k_x .)

To examine in more detail the form of the scaling function $\mathcal{Z}(\tau)$, we have regraphed in fig. 11 the computed data of fig. 10 as a log–log plot of $S(k_y)/y_{\text{coll}}$ versus $k_y y_{\text{coll}}$. At small τ , in the power-law regime, we know that $\mathcal{Z}(\tau) \sim 1/\tau^{2-\eta}$. For large τ , in the Lorentzian regime, $\mathcal{Z}(\tau) \sim \tau^{-2}$ before finite-size breakdown sets in. If \mathcal{Z} had a pure power-law form, this plot would consist of a straight line. Here, the slope expected from eq. (27) fits the data only up to $k_y \approx 4/y_{\text{coll}}$. Beyond that the slope decreases to a value consistent with $\eta_{\text{eff}} = 0$. This limiting form describes the com-

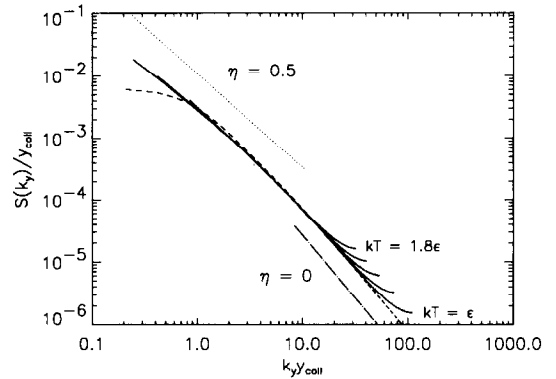


Fig. 11. Plot of logarithm of $S(k_y)$ versus the logarithm of k_y , showing the limited regime of power-law singularity. The dashed line shows the Gruber–Mullins approximation of eq. (25). The dotted line has a slope corresponding to $\eta_{\text{eff}} = 0.5$ (cf. fig. 5); the dash-dotted line has a slope corresponding to the prediction of a Lorentzian line shape $S(k_y) = 4b^2/k_y^2$ when k_y is large.

puted results accurately for $k_y y_{\text{coll}}$ greater than about ten.

Clearly, in making contact with experiment it is important to understand at what k_y does $S(k_y)$ become so small that it cannot be measured accurately. In a recent sensitive X-ray diffraction experiment [9], this k_y could be as small as 0.002 \AA^{-1} , where $S(k_y)$ dropped to three orders of

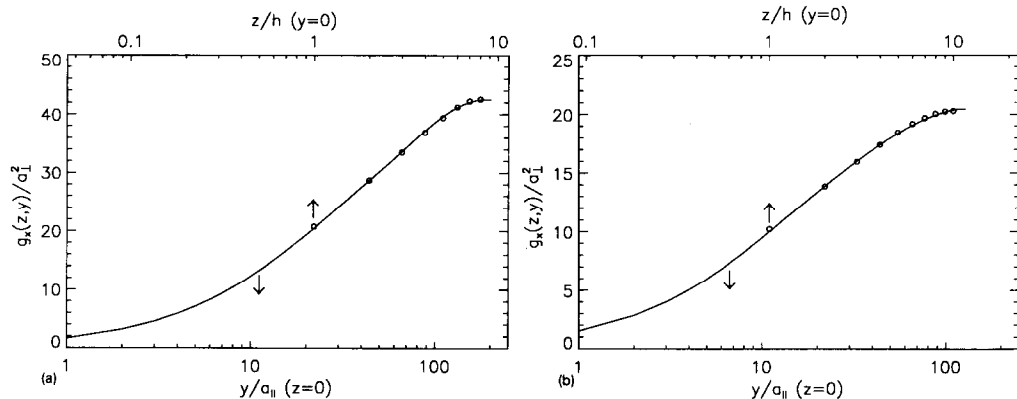


Fig. 12. This figure compares the step correlations along the step edge (solid lines, bottom abscissa) with those perpendicular to the step edges (circles, top abscissa) for (a) non-interacting steps, and for (b) steps interacting through a A/x^2 potential, with $A = 4k_B T a_{\parallel}$. In both cases the average terrace width l was $10a_{\perp}$, and $k_B T = \epsilon$. In (a) the coordinates perpendicular to the step edges were multiplied by a factor of 22 so as to bring the curves in the two directions together. This factor compares favorably with the value of ~ 17 suggested by eq. (28) for this temperature; in (b) this factor was divided by 2.18 as suggested by eq. (33).

magnitude below $S(0)$. Note, from eq. (27), that the size of $S(0)$ must be limited by (system-specific) finite-size effects, so that it is naive to assume that the simulated results become unobservable at the same value of $S(k_y)/S(0)$ as the experimental data does.

Recent experimental work [9] has successfully characterized the asymmetry of the peak in the power-law regime, i.e., the ratio c_x/c_y . In the free-fermion regime of widely spaced steps, this anisotropy has a distinctive form. To see this, consider the generalization of the correlation function of eq. (1), between step edges, $g_x(z, y) \equiv \langle [x(0, 0) - x(z, y)]^2 \rangle$, where the coordinate z labels the step edges. At large distances z or y , this correlation function has the form [17,18]:

$$g_x(z, y) \sim \frac{\eta l^2}{\pi^2} \ln \left[\left(\frac{z}{h} \right)^2 + \left(\frac{\pi k_B T y}{\tilde{\gamma} l^2} \right)^2 \right]. \quad (28)$$

It is straightforward [12] to show that eq. (28) leads to eq. (27) with

$$\frac{c_x}{c_y} = \frac{\tilde{\gamma} l}{\pi k_B T} = \frac{la_{\parallel}}{\pi b^2}. \quad (29)$$

Fig. 12a presents the results of a Monte Carlo simulation which approximately verifies eq. (28) for the simple TSK model at a temperature equal to the kink energy. As an application of this equation, we consider the recent measurements on vicinal Si(111) by Noh et al. [9] and Alfonso et al. [25]. For steps separated by 55 \AA , the observed value of c_x/c_y at 1120 K is ~ 3.9 . Using the estimate by Alfonso et al. for the step-edge stiffness at 1170 K of $1.1 \times 10^{-10} \text{ J m}^{-1}$, one finds from eq. (29), that c_x/c_y should be ~ 12 : the step-edge stiffness would have to be a factor of three smaller than estimated to give the observed ratio. Given that $\tilde{\gamma}$ is probably only determined up to an order of magnitude, failure of the non-interacting step picture for high-temperature Si(111) may not be ruled out on this basis. The role of step–step interactions on the asymmetry is discussed in the next section.

4. The role of energetic step–step interactions

Recent work on several different surfaces has shown that energetic interactions between steps

can be important [2,4,7,36–38] in understanding step structure of even small-angle vicinal surfaces. Thus, when interpreting diffraction profiles, one must consider how such interactions modify the simple picture painted above. Attention has focused on interactions due to elastic relaxations at the step edges. The magnitudes of these interactions are largely determined by the surface stress, which is known in only a few cases, so it is in general difficult to evaluate the applicability of the non-interacting step picture of the preceding sections. (We caution, however, that in general the step–step interactions can be expected to be much weaker than observed on Si(100), where the *anisotropic* stress of the (2×1) reconstruction causes asymptotic interactions to actually diverge.) Since computing the surface correlation functions with arbitrary step–step interactions is generally more difficult without interactions we will consider their effect within the Gruber–Mullins (single wandering step) framework, encouraged by this model's successes described in the preceding two sections. Suppose $U(x)$ is the potential, per unit length of the steps, between two steps separated by x . If $U(x)$ is sufficiently strongly repulsive (i.e., the temperature is low enough) that it strongly inhibits direct step collisions, then one might expect to approximate the potential felt by the wandering step by

$$\begin{aligned} V(x, l) &= U(l+x) + U(l-x) \\ &\approx 2U(l) + U''(l)x^2, \end{aligned} \quad (30)$$

where in the final form we have expanded about $x=0$. For this potential, correlations along the step edge are governed by harmonic oscillator eigenstates and eigenvalues within the formalism of eqs. (6)–(9). Again, one finds [23] that S is approximately Lorentzian with a correlation length given by an expression resembling eq. (26):

$$\xi(T, l) = 2a_{\parallel} \left(\frac{w}{b(T)} \right)^2. \quad (31)$$

Again, ξ is an effective distance between collisions, but with the average terrace width l replaced by the width w of the terrace-width distri-

bution, i.e., the root mean-square deviation of a single particle in a (1D) harmonic potential:

$$w = \sqrt{\langle x(y)^2 \rangle} = \left(\frac{k_B T b^2(T)}{8U''(l) a_{\parallel}} \right)^{1/4}. \quad (32)$$

As one increases the strength of step–step repulsions, w decreases, increasing the correlation length and decreasing the width of the diffraction profiles. With significant A/x^2 repulsions, the thermal scaling of the widths of these profiles, $\alpha \xi^{-1}$, varies as $bT^{-1/2}$ rather than b^2 . If, instead, $U(l) \propto \ln(l)$, then the scaling with respect to misorientation angle will change to $\xi^{-1} \propto l$, compared to l^2 in the free or A/x^2 case.

Eq. (31) can be expected to be a reasonable representation of the correlation length only when $w < l$. When the potential is so weak (or the temperature is so high) that w becomes comparable to l , the non-interacting expression of eq. (26) becomes appropriate. (If the temperature is so high that b is comparable to l or w , neither equation is valid.)

The above results suggest that, over most of the surface Brillouin zone, $S(k_y)$ for interacting steps will have the same general behavior as the non-interacting steps presented in the preceding section, except with eq. (31) replacing eq. (26). Of course, this Gruber–Mullins picture is only appropriate at large k_y , when the intensity quickly becomes too weak to be measured accurately: At smaller k_y the power-law divergence appears, and, as discussed by Saam [32], η will be different from the noninteracting case considered here. Indeed, η for interacting steps will be temperature dependent (and the rescaling of figs. 5 and 8 will fail): at low enough temperatures the power-law singularity can be replaced by a δ function – the vicinal surface can become a high-Miller index *facet* on the equilibrium crystal shape [39]. (In this case one would expect the Gruber–Mullins approximation for $S(k_y)$, with its δ function, to provide an even better account of the structure factor.)

The dependence of the aspect ratio c_x/c_y on T and l should also change when strong repulsions are present. To assess this effect, we suppose that the primary effect of the step repulsions

is simply to forbid small terrace widths. A natural gauge of this local inhibition is the terrace width distribution. If one simply scales *all* of the step fluctuations by the width of the distribution, instead of eq. (28) one has

$$g_x(z, y) = \frac{w^2(A)}{w^2(A=0)} \frac{l^2 \eta(A=0)}{\pi^2} \times \ln \left\{ \left(\frac{z}{h} \right)^2 + \left[\frac{w^2(A=0) \pi k_B T y}{w^2(A) \tilde{\gamma} l^2} \right]^2 \right\}. \quad (33)$$

To test this equation, we consider the special case of inverse square interaction with amplitude $\tilde{\gamma} A = 2(k_B T)^2$. The long-range correlations for this model are known exactly from the work of Sutherland [40]: the amplitude of the logarithm is exactly half of the non-interacting case. From previous numerical work [41] we know that w^2 is smaller by a factor of 2.18 than the free-fermion model, roughly verifying the prefactor of eq. (33). Fig. 12b tests the predictions of eq. (33) for the asymmetry. Notice that in this picture (and as confirmed by our simulations), step–step repulsions both decrease the value of η in eq. (33) and the asymmetry by the same amount. Since we have also shown previously that a reasonable approximation to w^2 is given by eq. (32), the influence of interactions on the profiles can be readily estimated. Of course, this analysis fails when the interactions become strong enough that the system approaches its roughening temperature, which can be expected to occur when w becomes on order of a_{\perp} . (This Lindemann-like criterion for the roughening temperature of vicinal surfaces is consistent with the analysis of ref. [12] – in particular, eq. (38) of ref. [12] amounts to $w(T_R) \approx a_{\perp}$, in our notation.)

As an application of eq. (33), we consider again the diffraction measurements of Noh et al. [9] on high-temperature Si(111). Alfonso et al. [25] have measured terrace width distributions on these surfaces. Analyzing steps spaced more than 200 Å apart, they find that $w \approx 0.33l$, compared to the free-fermion model result of $w \approx 0.42l$ [41], thus revealing repulsive step–step interactions. If one extrapolates this result down to the

55 Å separation studied by Noh et al., based on eq. (33) one would have expected a measured η of $(0.33/0.42)^2$ or 0.6 of the value of 0.5 for the free-fermion model. This deduction is in direct conflict with experiment [9], where η is observed to be 2.7 times as large as the free-fermion result [42]. This disagreement suggests that the result of Alfonso et al. for the terrace width distribution cannot be extrapolated down to small distances. Notice, however, following the discussion of the preceding section, that the factor of 0.6 change in the asymmetry of the spots predicted by eq. (33) causes the measured asymmetry to be closer to what one would expect from the measurement of Alfonso et al. for $\tilde{\gamma}$.

5. Conclusions and implications for analysis of experiments

We now make some observations about how one might analyze experimental diffraction data on the basis of the above analysis. The comparison of fig. 10 of the Gruber–Mullins model profiles with the Monte Carlo data suggests that one might attempt to fit $S(k_y)$ to a simple Lorentzian at large k_y . When the step–step interactions are weak, the correlation length one obtains from this fit can be simply interpreted in terms of the step diffusivity of eq. (2). Given a model for the kink Hamiltonian, the diffusivity can be used to extract estimates of the kink energy. We again caution, however, a Lorentzian will poorly approximate the profiles at small k_y ; indeed when one approaches the half width of the Lorentzian fit, the fit should fail.

An alternate procedure, outlined in an earlier publication [43], would use the fact that the entire shape of the scaled profile does not change with T . By experimentally determining the rescaling necessary to collapse the profiles onto a single curve, one would obtain a quantity proportional to $y_{\text{coll}}(l, T)$. An Arrhenius plot in the low-temperature limit, for example, of this quantity could then be used to estimate kink energies. (One should note, as shown in fig. 3, that the exponential dependence of y_{coll} on the temperature is

only true of high-symmetry directions.) This procedure has the advantage of using all of the information in the profiles, and not necessarily requiring complicated fits of the data. Also, as discussed in the preceding section, failure of the profiles to scale at small k_y , would be a signature of significant step interactions.

Another approach would involve using a technique such as STM to determine b and step interactions directly [2,4]. Then diffraction measurements of $\xi(T)$ could be used, through eqs. (26) and (31), to check that the temperature evolution is consistent with hypotheses of thermal equilibrium. (Since surface self-diffusion is usually limited at temperatures where conventional STM can be performed [3], it is by no means certain that equilibrium is being observed.)

The small range of k_y , where power-law line-shapes are evident in our calculations underscores the difficulty of determining η from experimental probes: only at length scales larger than the correlation length given by eq. (26) (or presumably eq. (31)) does the logarithmic behavior of stepped surfaces become apparent. Being able to distinguish the power-law behavior of a rough surface from a delta function plus Lorentzian of eq. (25) requires instrumental resolution much larger than ξ . (For example, given estimate for $\tilde{\gamma}$ of 10^{-10} J m⁻¹ by Alfonso et al. [25] for high-temperature Si(111), one would estimate y_{coll} of ~ 600 Å for the 3.3° vicinal Si(111) surfaces studied by X-ray diffraction by Noh et al. [9]; most low-energy electron diffraction instruments would have insufficient resolution to probe these length scales.)

The Gruber–Mullins model is used for other properties besides the transverse step-edge correlations. For example, it accurately gives the form of the orientational dependence of the increase of the surface free energy of vicinal surfaces [39,44]: at low temperatures the exact free energy per unit length *per step* (viz. l times that per area) has the form $f(l) = f(0) + b^2\pi^2/12l^2$ [44], compared to the Gruber–Mullins result (obtainable from E_0 given just after eq. (9)) of $f(l) = f(0) + b^2\pi^2/8l^2$. We have also found it to yield satisfactory estimates of terrace-width distributions [23,34]. Thus, it is a ready source of at least

semiquantitative information about vicinal surfaces.

An important issue which we have not addressed here is the question of whether it is reasonable to expect thermal equilibrium to be realized in experimental systems. Although it is reasonable that the local kink structure can equilibrate quickly, large length scale behavior equilibrates slowly (especially if the only mechanism is surface diffusion) [45]. Thus, one must exercise caution in attempting to interpret large length scale behavior in terms of equilibrium theories. (For example, a linear density of order merely $1/y_{\text{coh}}$ of quenched impurities along the step edge would presumably destroy the logarithmic divergence of step position correlation functions, making it difficult to observe experimentally [46].)

Acknowledgements

This work was supported in part by the NSF under grants DMR-89-18829 and 91-03031. Acknowledgement is also made to the Donors of the Petroleum Research Fund, administered by the American Chemical Society for the partial support of this research. We thank Drs. Jill Goldberg and R.J. Phaneuf for many helpful discussions, and Professor J.D. Weeks for providing computational facilities used for part of this study. We also acknowledge use of the facilities of the University of Maryland Computer Science Center.

Appendix

We consider here the height correlation function

$$g_z(y) \equiv \langle [z(y) - z(0)]^2 \rangle.$$

analyzed by Villain et al. [12]. Rather than measuring the meanderings of a step, this function gauges how many terraces apart are two points separated by y , but with the same value of x . At small y this is just the probability that the points are on neighboring terraces, i.e., that a step crosses between them. If we assume that the

probability of finding a step between x and $x + dx$ is just l^{-1} , then the chance is $l^{-1} \exp(-x_0/l)$ that the first step to the left of $(0, 0)$ lies at $(-x_0, 0)$. The chance that this step meanders to (x_y, y) , on the right of $(0, y)$, is Gaussian in the separation: $[2\pi g_x(y)]^{-1/2} \exp[-(x_0 + x_y)^2/2g_x(y)]$, where $g_x(y)$ denotes the mean-square separation. Thus, the overall probability of a step crossing from left of $(0, 0)$ to right of $(0, y)$ is the double integral (over both x_0 and x_y , each from 0 to ∞) of the product of these expressions. Expanding the resulting error function, using eq. (2), and multiplying by two since the step could just as well cross from the right of $(0, 0)$ to the left of $(0, y)$, we find

$$g_z(y) \sim \frac{bh^2}{l} \sqrt{\frac{2y}{\pi a_{\parallel}}}$$

as given in the text. This behavior is obviously qualitatively different from that of $g_x(y)$.

References

- [1] E.D. Williams and N.C. Bartelt, *Science* 251 (1991) 349.
- [2] B.S. Swartzentruber, Y.-W. Mo, R. Kariotis, M.G. Lagally and M.B. Webb, *Phys. Rev. Lett.* 65 (1990) 1913.
- [3] Although very recently there has appeared a report of successful STM at the elevated temperatures at which steps are mobile. S. Kitamura, T. Sato and M. Iwatsuki, *Nature* 351 (1991) 215.
- [4] X.-S. Wang, J.L. Goldberg, N.C. Bartelt, T.L. Einstein and E.D. Williams, *Phys. Rev. Lett.* 65 (1990) 2430.
- [5] M. Henzler, *Surf. Sci.* 22 (1970) 12.
- [6] P.R. Pukite, C.S. Lent and P.I. Cohen, *Surf. Sci.* 161 (1985) 39, and references therein.
- [7] R. Kariotis, B.S. Swartzentruber and M.G. Lagally, *J. Appl. Phys.* 67 (1990) 2848.
- [8] N.C. Bartelt, T.L. Einstein and E.D. Williams, *Surf. Sci.* 244 (1991) 149.
- [9] D.Y. Noh, K.I. Blum, M.J. Ramstad and R.J. Birgeneau, *Phys. Rev. B* 44 (1992) 10969.
- [10] J. Lapujoulade, J. Perreau and A. Kara, *Surf. Sci.* 129 (1983) 59.
- [11] E.H. Conrad, R.M. Aten, D.S. Kaufman, L.R. Allen, T. Engel, M. den Nijs and E.K. Riedel, *J. Chem. Phys.* 84 (1986) 1015.
- [12] J. Villain, D.R. Grempel and J. Lapujoulade, *J. Phys. F* 15 (1985) 809.
- [13] W. Selke and A.M. Szpilka, *Z. Phys. B* 62 (1986) 381;

- B. Salanon, F. Fabre, J. Lapujoulade and W. Selke, *Phys. Rev. B* 38 (1988) 7385.
- [14] D.A. Huse and M.E. Fisher, *Phys. Rev. B* 29 (1984) 239.
- [15] V.L. Pokrovsky and A.L. Talapov, *Theory of Incommensurate Crystals* (Harwood Academic, Chur, 1984).
- [16] S.G.J. Mochrie, A.R. Kortan, R.J. Birgeneau and P.M. Horn, *Phys. Rev. Lett.* 53 (1984) 985; S.G.J. Mochrie, A.R. Kortan, P.M. Horn and R.J. Birgeneau, *Phys. Rev. Lett.* 58 (1987) 690.
- [17] H.J. Schulz, *Phys. Rev. B* 22 (1980) 5274.
- [18] J. Villain and P. Bak, *J. Phys. (Paris)* 42 (1981) 657.
- [19] M.E. Fisher and D.S. Fisher, *Phys. Rev. B* 25 (1982) 3192.
- [20] W. Kossel, *Nachr. Ges. Wiss. Göttingen* 135 (1927).
- [21] E.E. Gruber and W.W. Mullins, *J. Phys. Chem. Solids* 28 (1967) 875.
- [22] M.E. Fisher, *J. Stat. Phys.* 34 (1984) 667; in: *Fundamental Problems in Statistical Mechanics VI*, Ed. E.G.D. Cohen (North-Holland, Amsterdam, 1985) p. 1.
- [23] N.C. Bartelt, T.L. Einstein and E.D. Williams, *Surf. Sci. Lett.* 240 (1991) L591.
- [24] This is the same correlation function $g(z, y)$ defined in ref. [8], with z implicitly fixed at zero, so that only the correlations along one particular step edge are examined.
- [25] C. Alfonso, J.M. Bermond, J.C. Heyraud and J.J. Métois, *Surf. Sci.* 262 (1992) 371.
- [26] M. Mundschau, E. Bauer, W. Telieps and W. Świąch, *Surf. Sci.* 223 (1989) 413.
- [27] Z. Zhang, Y.-T. Lu and H. Metiu, *Surf. Sci. Lett.* 259 (1991) L719; They suggest that kink-kink interactions are needed to obtain adequate accounting of data on kink-length and -width distributions in ref. [2]. (However, no such need is found by B. Swartzentruber, private communication.)
- [28] S.T. Chui and J.D. Weeks, *Phys. Rev. B* 14 (1976) 4978.
- [29] H. van Beijeren, *Phys. Rev. Lett.* 38 (1977) 993.
- [30] M. den Nijs, in: *Phase Transitions*, Eds. C. Domb and J.L. Lebowitz, Vol. 12 (Academic Press, New York, 1988).
- [31] R.P. Feynman, *Rev. Mod. Phys.* 20 (1948) 367.
- [32] W.F. Saam, *Phys. Rev. Lett.* 62 (1989) 2636.
- [33] L.K. Warman III, N.C. Bartelt and T.L. Einstein, unpublished.
- [34] B. Joós, T.L. Einstein and N.C. Bartelt, *Phys. Rev. B* 43 (1991) 8153.
- [35] H. van Beijeren and I. Nolden, in: *Structure and Dynamics of Solid Surfaces II*, Eds. W. Schommers and P. von Blanckenhagen (Springer, Berlin, 1987) p. 259; P. Nozières, in: *Solids far from Equilibrium*, Ed. C. Godrèche (Cambridge University Press, Cambridge, 1992) p. 1.
- [36] O.L. Alerhand, A.N. Berker, J.D. Joannopoulos, D. Vanderbilt, R.J. Hamers and J.E. Demuth, *Phys. Rev. Lett.* 64 (1990) 2406.
- [37] G.P. Kochanski, *Phys. Rev. B* 41 (1990) 12334.
- [38] J. Frohn, M. Giesen, M. Poensgen, J.F. Wolf and H. Ibach, *Phys. Rev. Lett.* 67 (1991) 3543.
- [39] M. Wortis, in: *Chemistry and Physics of Solid Surfaces VII*, Eds. R. Vanselow and R. Howe (Springer, Berlin, 1988) p. 235.
- [40] B. Sutherland, *J. Math. Phys.* 12 (1971) 246, 251; *Phys. Rev. A* 4 (1971) 2019.
- [41] B. Joós, T.L. Einstein and N.C. Bartelt, *Phys. Rev. B* 43 (1991) 8153.
- [42] Notice that Noh et al. [9] did not measure diffraction profiles at the standard "out-of-phase" condition used in the low-energy electron diffraction literature. Because of the dependence of η on incident energy [12], the η_1 of ref. [9] should be $\frac{4}{9}$ as large as the value of η defined in this paper.
- [43] T.L. Einstein, N.C. Bartelt, J.L. Goldberg, B. Joós, X.S. Wang and E.D. Williams, in: *The Structure of Surfaces III*, Eds. S.Y. Tong, M.A. Van Hove, K. Takayanagi and X.D. Xie (Springer, Berlin, 1991) p. 486.
- [44] C. Jayaprakash, C. Rottman and W.F. Saam, *Phys. Rev. B* 30 (1984) 6549.
- [45] N.C. Bartelt, J.L. Goldberg, T.L. Einstein and E.D. Williams, *Surf. Sci.* 273 (1992) 252.
- [46] H. Ibach, private communication.